NASA/TM—2009-215645

Characterization of Damage in Triaxial Braid Composites Under Tensile Loading

Justin D. Littell and Wieslaw K. Binienda
The University of Akron, Akron, Ohio

Gary D. Roberts and Robert K. Goldberg
Glenn Research Center, Cleveland, Ohio

May 2009

NASA STI Program . . . in Profile

Since its founding, NASA has been dedicated to the advancement of aeronautics and space science. The NASA Scientific and Technical Information (STI) program plays a key part in helping NASA maintain this important role.

The NASA STI Program operates under the auspices of the Agency Chief Information Officer. It collects, organizes, provides for archiving, and disseminates NASA's STI. The NASA STI program provides access to the NASA Aeronautics and Space Database and its public interface, the NASA Technical Reports Server, thus providing one of the largest collections of aeronautical and space science STI in the world. Results are published in both non-NASA channels and by NASA in the NASA STI Report Series, which includes the following report types:

- TECHNICAL PUBLICATION. Reports of completed research or a major significant phase of research that present the results of NASA programs and include extensive data or theoretical analysis. Includes compilations of significant scientific and technical data and information deemed to be of continuing reference value. NASA counterpart of peer-reviewed formal professional papers but has less stringent limitations on manuscript length and extent of graphic presentations.

- TECHNICAL MEMORANDUM. Scientific and technical findings that are preliminary or of specialized interest, e.g., quick release reports, working papers, and bibliographies that contain minimal annotation. Does not contain extensive analysis.

- CONTRACTOR REPORT. Scientific and technical findings by NASA-sponsored contractors and grantees.

- CONFERENCE PUBLICATION. Collected papers from scientific and technical conferences, symposia, seminars, or other meetings sponsored or cosponsored by NASA.

- SPECIAL PUBLICATION. Scientific, technical, or historical information from NASA programs, projects, and missions, often concerned with subjects having substantial public interest.

- TECHNICAL TRANSLATION. English-language translations of foreign scientific and technical material pertinent to NASA's mission.

Specialized services also include creating custom thesauri, building customized databases, organizing and publishing research results.

For more information about the NASA STI program, see the following:

- Access the NASA STI program home page at *http://www.sti.nasa.gov*

- E-mail your question via the Internet to *help@sti.nasa.gov*

- Fax your question to the NASA STI Help Desk at 301–621–0134

- Telephone the NASA STI Help Desk at 301–621–0390

- Write to:
  NASA Center for AeroSpace Information (CASI)
  7115 Standard Drive
  Hanover, MD 21076–1320

NASA/TM—2009-215645

Characterization of Damage in Triaxial Braid Composites Under Tensile Loading

Justin D. Littell and Wieslaw K. Binienda
The University of Akron, Akron, Ohio

Gary D. Roberts and Robert K. Goldberg
Glenn Research Center, Cleveland, Ohio

National Aeronautics and
Space Administration

Glenn Research Center
Cleveland, Ohio 44135

May 2009

Trade names and trademarks are used in this report for identification only. Their usage does not constitute an official endorsement, either expressed or implied, by the National Aeronautics and Space Administration.

Level of Review: This material has been technically reviewed by technical management.

Available from

NASA Center for Aerospace Information
7115 Standard Drive
Hanover, MD 21076–1320

National Technical Information Service
5285 Port Royal Road
Springfield, VA 22161

Available electronically at http://gltrs.grc.nasa.gov

Characterization of Damage in Triaxial Braid Composites Under Tensile Loading

Justin D. Littell and Wieslaw K. Binienda
The University of Akron
Akron, Ohio 44325

Gary D. Roberts and Robert K. Goldberg
National Aeronautics and Space Administration
Glenn Research Center
Cleveland, Ohio 44135

Summary

Carbon fiber composites utilizing flattened, large tow yarns in woven or braided forms are being used in many aerospace applications. Their complex fiber architecture and large unit cell size present challenges in both understanding deformation processes and measuring reliable material properties. This report examines composites made using flattened 12k and 24k standard modulus carbon fiber yarns in a 0°/+60°/–60° triaxial braid architecture. Standard straight-sided tensile coupons are tested with the 0° axial braid fibers either parallel with or perpendicular to the applied tensile load (axial or transverse tensile test, respectively). Nonuniform surface strain resulting from the triaxial braid architecture is examined using photogrammetry. Local regions of high strain concentration are examined to identify where failure initiates and to determine the local strain at the time of initiation. Splitting within fiber bundles is the first failure mode observed at low to intermediate strains. For axial tensile tests splitting is primarily in the ±60° bias fibers, which were oriented 60° to the applied load. At higher strains, out-of-plane deformation associated with localized delamination between fiber bundles or damage within fiber bundles is observed. For transverse tensile tests, the splitting is primarily in the 0° axial fibers, which were oriented transverse to the applied load. The initiation and accumulation of local damage causes the global transverse stress-strain curves to become nonlinear and causes failure to occur at a reduced ultimate strain. Extensive delamination at the specimen edges is also observed.

Introduction

Composites that utilize large-tow-size yarns in automated manufacturing processes can offer the best combination of cost and performance for many aerospace structures. One example is the recent development of composite fan cases for jet engines in which large-unit-cell-size triaxial braid preforms are utilized with various resin infusion processes. Characterization of these braided materials is complicated by the nonuniformity of deformation within the unit cell as well as the possibility of edge effects related to the large size of the unit cell when standard straight-sided coupon specimens are used. Standard composite test methods (Ref. 1) are often used for unidirectional or balanced laminates, and there are material property databases (Refs. 2 to 4) available for these types of composite materials. However, there are no specific guidelines for use of the standard test methods with triaxial braid composites, and existing databases do not include data for these materials. Some guidance on specimen design and measurement techniques is available from research publications. Masters and coworkers (Refs. 5 to 8) have done extensive testing on braided materials and have proposed guidelines for strain gage size selection and specimen geometries. Tsotsis (Ref. 9) examined strain concentration around holes in open-hole tension specimens. While these reports provide guidance on adapting standard test methods for use with braided materials, they do not address the need to explore the nonuniform deformation within a unit cell. Optical measurement techniques have been used to explore such local deformation in various

materials. Grediac (Ref. 10) gives an overview of several techniques including speckle photography, image correlation, geometric Moiré, Moiré interferometry, and electronic speckle pattern interferometry. Some of these techniques have been applied to composite materials. Gliesche et al. (Ref. 11) used image correlation to measure deformation during tensile and in-plane shear tests of ±45° woven fabric. Local strains were averaged over an arbitrary section to provide an average strain, but local strain concentrations were not examined in detail. Other researchers have used Moiré interferometry to measure the surface deformations on composite materials in Iosipescu shear testing for validation and correlation of finite element models (Ref. 12). Similarly, using Moiré interferometry, Masters (Ref. 6) noticed a significant amount of heterogeneity on the surface of the specimen but did not discuss its possible influence on failure mechanisms and strength. Hale (Ref. 13) used Moiré interferometry to examine strains on woven laminate edges and concluded that Moiré interferometry was extremely sensitive to the heterogeneity on the free edge and fiber misalignment between the layers of lamina. He also mentions that Moiré interferometry is a valuable tool for measuring surface strains on the faces of laminates. Hubner et al. (Ref. 14) developed a full-field photoelastic surface coating technique for use on a composite tensile specimen that has a notch. Fergusson et al. (Ref. 15) used optical measurement techniques to determine strain fields on composite sandwich structures under four-point flexure.

In this paper, local deformation and failure in triaxial braid composite materials during tensile loading is examined using digital image correlation methods. One fiber architecture is examined with three different matrix materials. The material systems are representative of the types of materials that are being considered for use in jet engine components. Results of this investigation provide insight into the effect of local deformation and failure on global response and provide guidance for adapting standard coupon test methods for triaxial braid composites.

Experimental Methods

Materials

Composite materials were fabricated by resin transfer molding (RTM) using the high-strength, standard-modulus carbon fiber TORAYCA T700S (Toray Carbon Fibers America, Inc.) with three different 177 °C (350 °F) cure epoxy resins. Fiber properties reported by the fiber manufacturer are shown in Table I.

TABLE I.—FIBER PROPERTIES

Fiber	Tensile strength, MPa (ksi)	Young's modulus, Gpa (msi)	Failure strain, percent	Density, g/cm^3 (lb/in^3)
T700S	4900 (711)	230 (33.4)	2.1	1.80 (0.065)

Resins were selected to provide a range of toughness in the cured composites: (1) CYCOM PR 520 (Cytec Industries, Inc.) is a one-part toughened resin specifically designed for the RTM process. (2) CYCOM 5208 (Cytec Industries, Inc.) is a one-part untoughened resin. This resin is not specifically marketed as an RTM resin, but its flow characteristics are suitable for RTM. (3) The EPIKOTE™ Resin 862/EPIKURE™ Curing Agent W system (Resolution Performance Products, now Hexion Specialty Chemicals) is a two-part, low-viscosity system that is easy to process because of its low viscosity and long working life at room temperature. This resin system will be designated E–862 in this paper. Table II lists the cured resin properties reported by each manufacturer. These properties are representative values

TABLE II.—RESIN PROPERTIES

Resin	Tensile strength, MPa (ksi)	Young's modulus, GPa (msi)	Density, g/cm^3 (lb/in^3)
PR520	82 (11.9)	4.00 (0.58)	1.256 (0.045)
5208	50 (7.3)	3.8 (0.56)	1.265 (0.046)
E–862	61 (8.8)	2.7 (0.39)	1.200 (0.043)

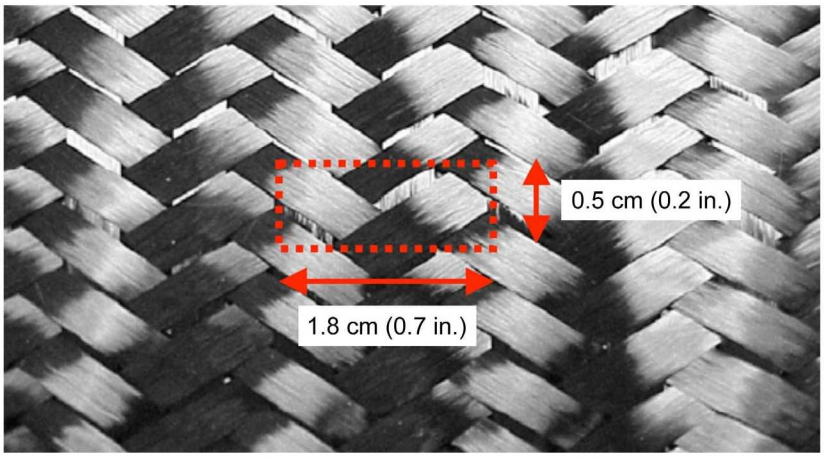

Figure 1.—Two-dimensional triaxial braid architecture.

only since actual properties depend on the cure and postcure conditions used for various applications as well as the test specimen geometry, temperature, and strain rate. A more complete set of tension, compression, and shear data at various strain rates and temperatures for the E–862 system is presented by Littell et al. (Ref. 16). Additional data on other resin systems is given by Littell (Ref. 17).

The two-dimensional triaxial braid preforms were fabricated by A&P Technology. The fiber architecture was a 0º/+60º/–60º triaxial braid. The 0° axial fibers were 24k flattened tows while the ±60° bias fibers were 12k flattened tows. (The terms 24k and 12k refer to the number of fibers in the fiber tow.) Although larger fiber bundles were used in the axial direction, the fiber bundle spacings in the axial and bias directions were adjusted to give the same fiber volume in the axial and bias directions. Because of the quasi-isotropic in-plane fiber architecture, the in-plane stiffness is expected to be the same in all directions. A picture of the braid architecture is shown in Figure 1. A unit cell of the braid architecture is indicated by the red rectangle. A unit cell is the smallest repeating geometry of a composite material that can represent the composite fiber architecture. In Figure 1 the ±60° bias fibers are visible on the surface. Portions of the 0° axial fibers that lie below the ±60° bias fibers can be seen in the open spaces between the ±60° bias fibers. Composite panels were fabricated by North Coast Composites. Six layers of the 0º/+60º/–60º braid were used to make a composite panel. Each of the six layers were placed into the RTM mold with the 0° fibers aligned in the same direction. Resin was then injected into the closed mold and cured according to processing conditions recommended by the resin manufacturer. Cured panel dimensions (after trimming) were 0.6096 m (2 ft) wide by 0.6096 m (2 ft) long by 0.3175 cm (0.125 in.) thick. Fiber volume of the cured composites was measured using the acid digestion technique. The T700S/PR520 composite had a fiber volume of 55.9±0.18 percent, the T700S/5208 composite had a fiber volume of 53.0±3.3 percent, and the T700S/E–862 composite had a fiber volume of 55.6±2.42 percent.

Specimen Geometries

Tensile test specimens were cut from the panels using an abrasive waterjet technique. Straight-sided tensile test specimens were prepared in accordance with ASTM D–3039. Specimens of 30.48 cm (12 in.) length by 3.578 cm (1.409 in.) width were used for the tensile tests. These dimensions were chosen so that the width contained at least two unit cells and the length conformed to ASTM length to width ratios. The tensile specimens were cut in two orientations. For the axial tensile test, the 0° braid fibers lie along the longitudinal axis of the specimen and parallel to the direction of applied load. For the transverse tensile test the 0° braid fibers lie perpendicular to the longitudinal axis of the specimen, and perpendicular to the direction of applied load.

Test Equipment

All specimens were tested in a hydraulically actuated, 220-kN (50-kip) test machine. Tests were conducted under displacement control with a displacement rate of 0.635 mm/min (0.025 in./min). Strain measurements were made by photogrammetry using a digital image correlation system manufactured by GOM (Ref. 18). Load measurements from the test rig were input to the GOM system to generate the stress-strain curves. The digital image correlation technique is similar to the one described in Littell et al. (Ref. 17). A brief summary is provided here to familiarize the reader with the technique. Two cameras are connected to a computer equipped with software capable of pattern recognition and calculation of position from stereo images. A calibration procedure is performed in which a series of images of known dimensions are placed in the intersecting field of view of the two cameras, and the location of the image is mapped by the software. This results in a calibrated volume of space that can be used for tracking displacement of test specimens under load. The test specimen is painted with a speckle pattern for optimum pattern recognition. A three-dimensional map of the specimen surface is obtained before the specimen is loaded. The specimen is then loaded, and the pattern recognition software is able to track the three-dimensional displacement of any point which remains in the initial field of view. Strain is then calculated from surface displacements measured at specified time intervals during a test. Stress-strain curves are calculated from the synchronized load and strain measurements.

Results

Global Stress-Strain Data

Figure 2 shows an example of the axial strain field measured at one specific time step during an axial tensile test. The field of view captures the entire 3.578-cm (1.409-in.) specimen width and approximately 5.08 cm (2 in.) of the specimen height. The strain field in Figure 2 is nonuniform and shows high strain regions within the braid architecture that can become sites for local damage. An average strain can be calculated by averaging the nonuniform strain within a particular field of view, or by tracking the location

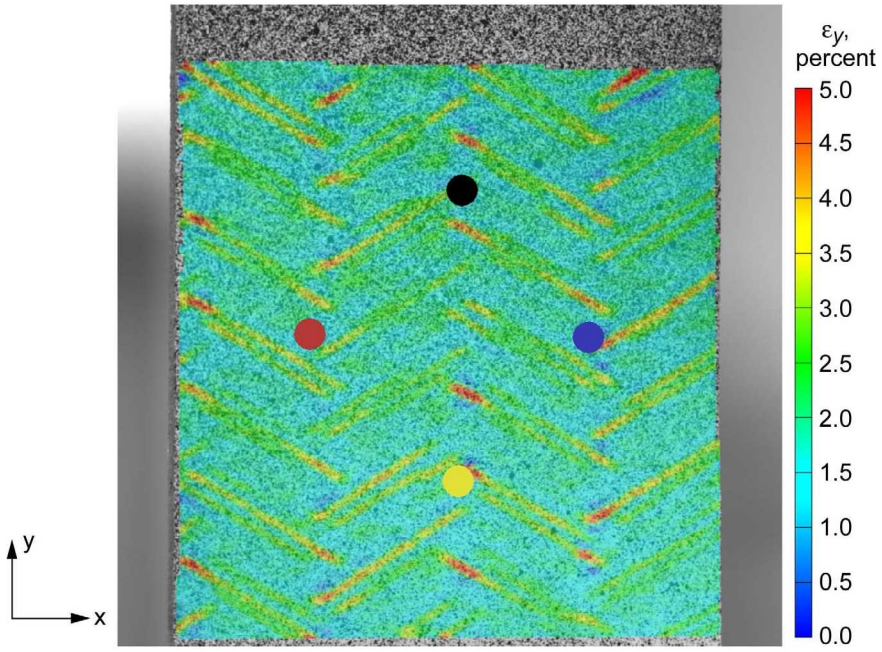

Figure 2.—Typical axial strain field ε_y in axial tensile test. Colored dots indicate points used for global strain calculations in axial and transverse directions.

of specific points. A potential problem with the averaging approach is that the calculated strain can be affected by unrealistically high strain values and possible loss of pattern recognition at local damage sites. To avoid this complication, global strain was measured by tracking specific points that are separated by a distance that is large compared to the size of the local damage. The locations of these points, which are approximately 1.905 cm (0.75 in.) apart, are indicated in Figure 2. The two points aligned along the specimen axis are used to calculate axial strain, and the two points aligned transverse to the specimen axis are used to calculate transverse strain. Global strains are calculated by dividing the relative displacement between the two points in the loaded condition by their original separation in the unloaded condition. The distance of 1.905 cm (0.75 in.) selected for this work is in agreement with guidelines proposed by Masters (Ref. 6). Global strains in the axial and transverse directions were used to calculate a global Poisson's ratio. Representative global stress-global strain curves for the three composite material systems are shown in Figures 3 to 5.

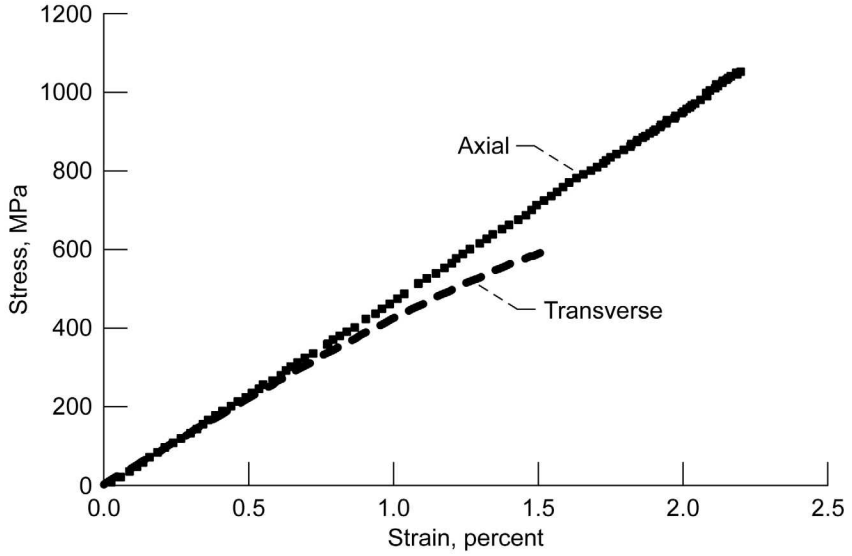

Figure 3.—Global stress versus global strain for T700S/PR520 material system.

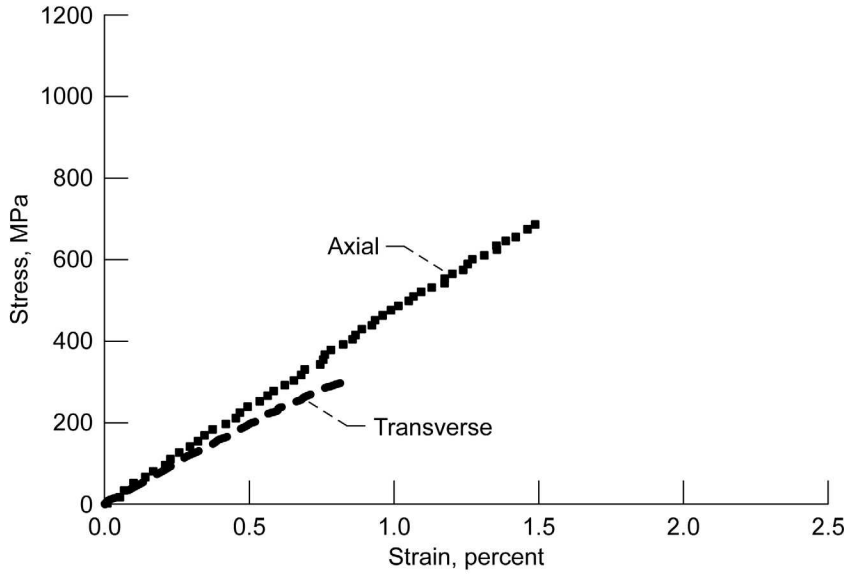

Figure 4.—Global stress versus global strain for T700S/5208 material system.

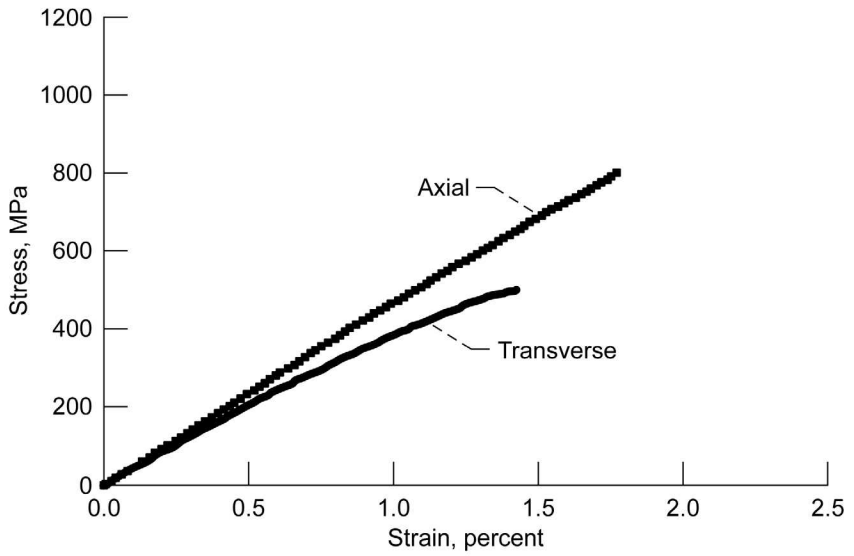

Figure 5.—Global stress versus global strain for T700S/E–862 material system.

TABLE III.—COMPOSITE MATERIAL PROPERTIES[a]

Material (fiber/resin)	Axial direction				Transverse direction			
	Strength, MPa (ksi)	Young's modulus, GPa (msi)	Failure strain, percent	Poisson's ratio	Strength, MPa (ksi)	Young's modulus, GPa (msi)	Failure strain, percent	Poisson's ratio
T700S/PR520	1035±34 (150±4.9)	47.6±1.1 (6.9±0.2)	2.16±0.09	0.31±0.02	599±3 (87±0.4)	42.8±1.6 (6.2±0.2)	1.68±0.19	[b]0.30±0.003
T700S/5208	693±46 (100±6.7)	47.0±1.0 (6.8±0.1)	1.5±0.09	0.29±0.03	310±15 (45±2.1)	41.4±4.5 (6.0±0.7)	0.85±0.05	0.27±0.006
T700S/E–862	800±6 (116±0.9)	46.9±1.6 (6.8±0.2)	1.78±0.08	0.30±0.03	462±36 (67±5.2)	41.6±1.3 (6.0±0.2)	1.44±0.09	0.29±0.02

[a]Error limits indicate one standard deviation.
[b]Average value for two tests.

Material modulus was calculated from the slope of the curve in the region from 0 to 0.2 percent strain. Since a measurement point was not always available at exactly 0.2 percent strain, the closest data point to 0.2 percent was used for the calculation. Table III shows the moduli, strengths, failure strains, and Poisson's ratios for the three material systems. A minimum of five tests were conducted in each direction for each material system. The average values are shown in Table III.

Although the fiber architecture is quasi-isotropic, the transverse moduli are slightly less than the axial moduli. This small difference could be a result of many factors including greater undulation of bias fibers compared with the axial fibers or a slight deviation of fiber angles or fiber volumes. The toughened material system, T700S/PR520, had the highest strength in both the axial and transverse directions, whereas the untoughened system, T700S/5208, had the weakest strength in both directions. The axial failure strain of T700S/PR520 was 2.16 percent, which is close to the expected failure strain of 2.1 percent indicated in Table I for the T700S fiber. Despite the local stress concentrations shown in Figure 2, the axial fibers are able to be fully loaded when the toughened matrix material is used. The axial failure strains for composites made using the untoughened matrix materials were significantly less than the T700S fiber failure strain. The reduced failure strains for these composites is an indication that local strain concentrations like those shown in Figure 2 limit the ability of the composite to take full advantage of the strain capability of the axial fibers. The axial stress-strain curve for the toughened T700S/PR520 system in Figure 3 is nearly linear until failure whereas the axial stress-strain curves for the untoughened systems in Figures 4 and 5 become slightly nonlinear at strains approaching the failure strain. A possible

cause of this deviation from linearity is local damage initiation, and methods to explore this type of local damage will be discussed later in this paper.

For specimens tested in the transverse direction there are no continuous fibers that extend from the top grip to the bottom grip through the entire length of the specimen in the direction of loading. Instead, the axial braid fibers are transverse to the loading direction and terminate on the edge of the specimen. The measured transverse tensile strength is much lower than the measured axial tensile strength for all material systems, as shown in Table III. The transverse stress-strain curves in Figures 3 to 5 become nonlinear at low strains. The toughened material system shows less reduction in strength and greater strain before the onset of nonlinearity. The cause of this nonlinearity and the effect of the matrix material on strength are examined in more detail in later sections of this paper. In contrast to the effect of material toughness on strength, there appears to be little effect on stiffness. This behavior is reasonable since stiffness is measured at low strains, where the effects of damage are small, and stiffness is controlled primarily by the fiber architecture.

Full-Field Strain Overlay Method

A possible cause for the nonlinear behavior mentioned above is damage resulting from local strain concentration within a unit cell. Figure 2 shows an example of the occurrence of local strain concentrations. Since specimens used for photogrammetry are painted with a speckle pattern, it is not possible to locate the site of strain concentration within the braid architecture without further image processing. This section describes a method that was developed to locate the sites of high strain concentration. An image overlay technique was developed to overlay the strain map onto a digital image of the braid architecture. Figure 6 illustrates the overlay technique using a T700S/PR520 axial tensile specimen.

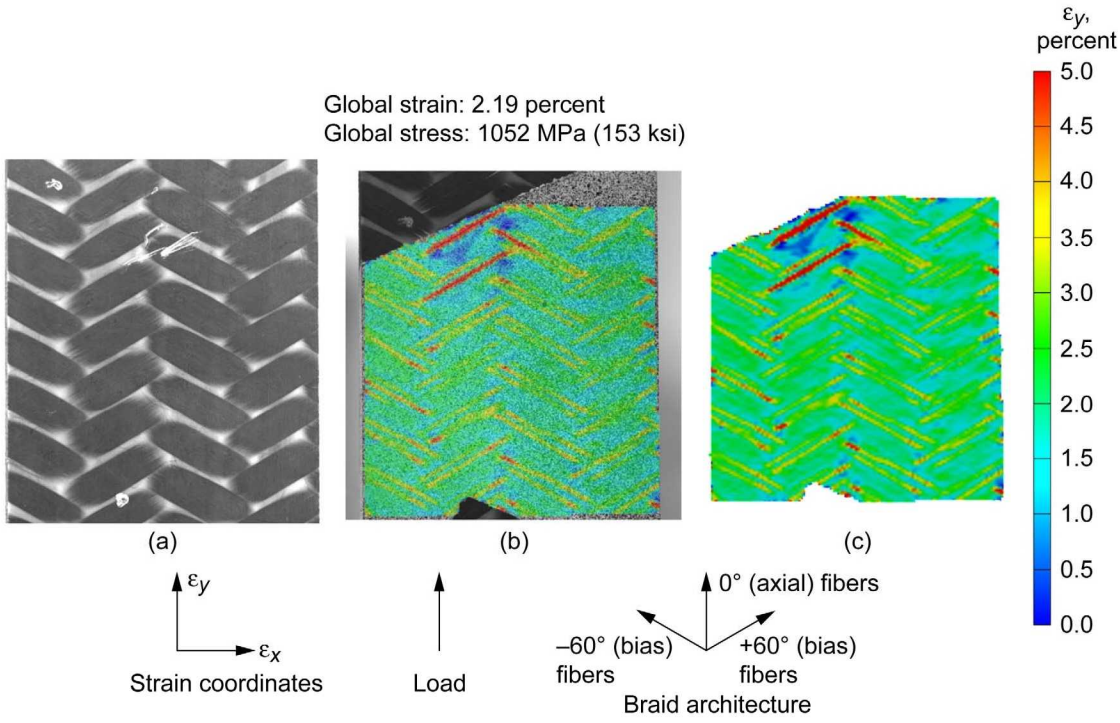

Figure 6.—Overlay technique illustrated using axial tensile test on T700S/PR520 material system. (a) Digital image of specimen before painting. (b) Postprocessed strain data on painted specimen. (c) Postprocessed strain data only.

Figure 6(a) shows a digital image of the unpainted specimen before the speckle pattern is applied. Figure 6(b) shows postprocessed strain data mapped onto the painted specimen, and Figure 6(c) shows the postprocessed strain data only. In the overlay technique, image (b) is first mapped onto (a) by matching the visible fiber locations. Then image (c) is mapped onto (b) by matching strain results. Image (b) is then removed, leaving the final overlay with (a) and (c) only. Finally, the opacity of part (c) is reduced so that the fibers in (a) are visible. Figure 7 shows the final overlay picture used to determine locations of high strain on the surface of the specimen.

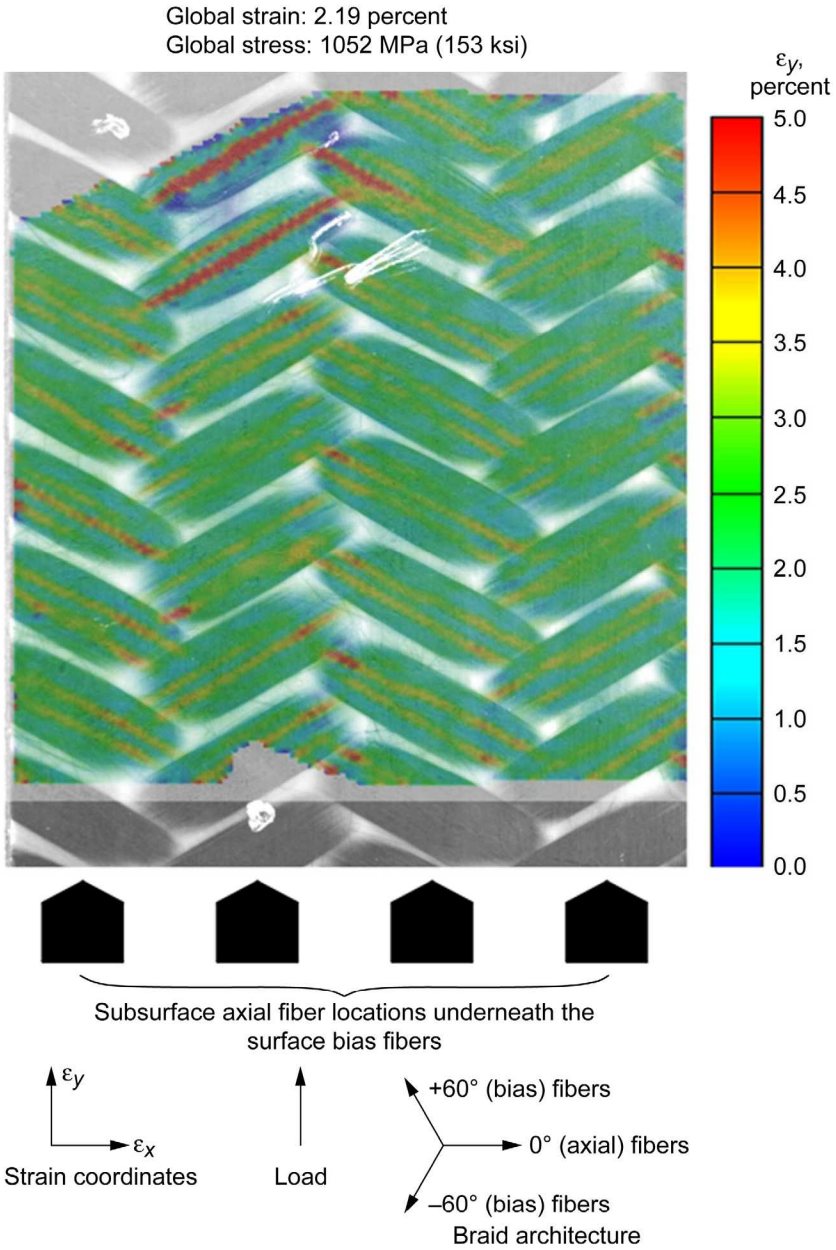

Figure 7.—Axial strain overlay on axial tensile specimen of T700S/PR520 material system.

The white regions in Figure 7 are resin-rich areas. These regions appear white because of the reduced opacity of the colored strain map. The white color does not indicate the strain level in these regions. However, the images in Figure 6 do not indicate any strain concentration pattern corresponding to the resin-rich areas. The green areas of Figure 7 indicate that the strain in most of the specimen is close to the global strain of 2.19 percent. The yellow and red lines in Figure 7 indicate that there are regions of high strain concentration within the fiber bundles on the surface of the specimen. The occurrence of splitting within fiber bundles was confirmed by optical and scanning electron microscopy (SEM). Fiber bundles were examined after testing for all of the material systems. Both surface fiber bundles and interior fiber bundles were examined. Figure 8 shows an example of fiber bundle splits (arrows) in a +60° bias fiber bundle extracted from the interior of a T700S/5208 axial tensile specimen after testing.

Quantitative measurements of the number of fiber splits were not made. However, the onset of splitting and the amount of splitting appeared to be similar for surface and interior fiber bundles. This suggests that the surface strain maps are a reasonable representation of the strain field in all 0°/+60°/–60° braid lamina layers of the composite. If the assumption is made that the surface strain field does actually represent the strain field in the interior, then the surface measurements can be used to deduce in situ material properties such as the transverse tensile failure strain of fiber bundles. A micromechanics analysis that utilizes these in situ property measurements has been recently developed (Ref. 17).

Figure 7 shows the splits that occur in surface bias fiber bundles during an axial tensile test. In this test the composite is loaded along the direction of the subsurface axial fibers. Figure 9 shows a similar overly for a transverse tensile test in which the load is applied perpendicular to the subsurface axial fibers.

In the transverse tensile test, splits occur in the subsurface axial fiber bundles. The effect of these subsurface fiber bundle splits are visible in the strain overlay shown in Figure 9. The small red horizontal lines that are visible between the surface bias fiber bundles are high local surface strains caused by splitting of the subsurface axial fiber bundles. Microscopy was performed to confirm that these regions of high local strain were a result of the subsurface fiber bundle splits and not surface cracking of the resin. In addition, microscopic examination indicated that the onset of splitting and the amount of splitting appeared to be similar for axial fiber bundles near the surface and in the interior of the composite. Figure 10 shows an edge view of a transverse tensile specimen. The areas of dark grey represent the axial fibers (running normal to the view in Fig. 10), while the areas of white represent the bias fibers. The circled areas in Figure 10 show the fiber bundle splits that occur in the axial fibers.

If the assumption is made that the surface strain field represents the strain field in the interior for all layers, then local stress-strain measurements at the sites of axial bundle splitting can be used to deduce the in situ transverse failure strain for the axial fiber bundles.

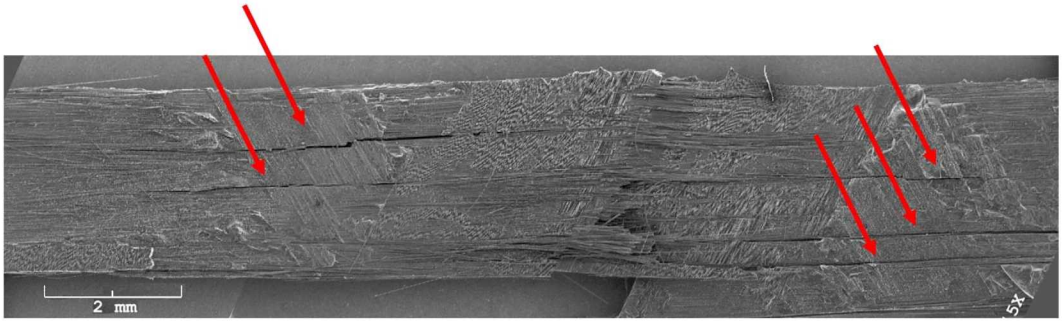

Figure 8.—Scanning electron microscopy (SEM) picture of bias fiber bundle extracted from T700S/5208 composite (25× magnification). Arrows indicate splitting within bundle.

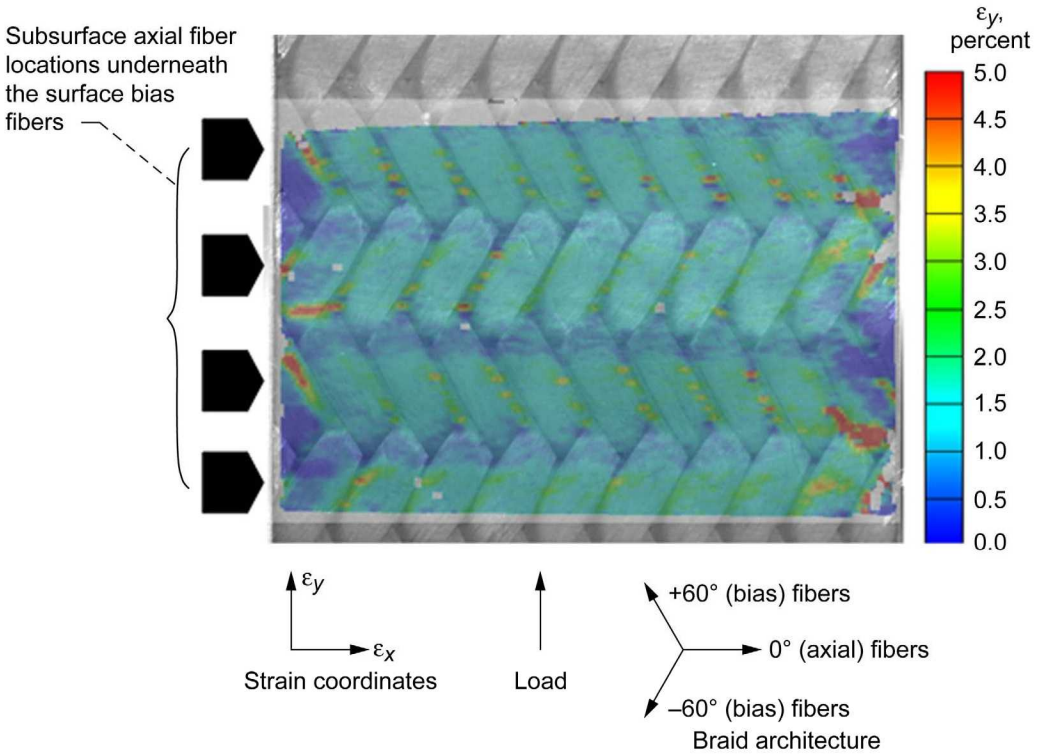

Figure 9.—Axial strain overlay on representative transverse tensile specimen of T700S/E–862 material system.

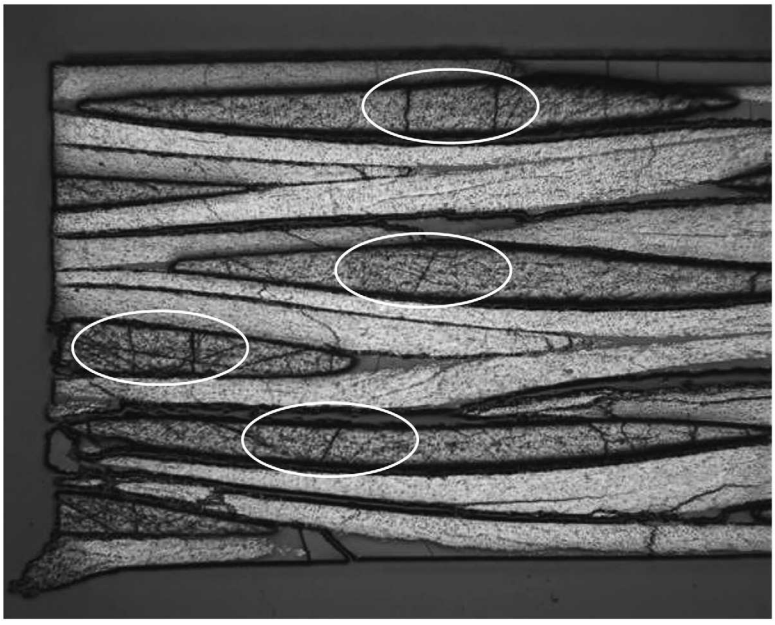

Figure 10.—Digital optical microscopic image showing splits in axial fiber bundles of transverse tensile specimen.

Local Deformation in Transverse Tensile Tests

Previous sections showed the global stress-strain response for three material systems and demonstrated a strain overlay technique that was developed to determine the locations of local high strain regions relative to the braid architecture. The remaining sections of this paper explore the local deformation in these high strain regions in more detail and examine differences for toughened and untoughened material systems. Figure 11 shows the axial surface strain in a transverse tensile test for the toughened T700S/PR520 material system at a load approaching the ultimate failure load.

The blue triangular regions at the edges of the specimen are areas that are not carrying load, as a result of localized edge damage. The extent of these edge effects demonstrates a deficiency in the use of standard straight-sided coupons for measuring material properties of the large-unit-cell-size triaxial braid materials considered in this paper. The global stress-strain curves measured using straight-sided coupons provide artificially low strength and stiffness values because of the edge effects. Alternative specimen designs have been proposed to eliminate the edge effects. One alternative is a bowtie specimen geometry (C.L. Bowman, "Mechanical Properties of Triaxial Braid Carbon/Epoxy Composites." Presented at the 35th International SAMPE Technical Conference—Materials and Processing: Enabling Flight…Our Legacy and Future, Dayton, Ohio, 2003) in which all of the axial and bias fibers in the gage section are gripped during a test. Another alternative is a tubular specimen geometry in which there are no edge terminations. Future work is planned to examine the advantages and disadvantages of various specimen geometries. In spite of the edge effects, data from tests using the standard straight-sided coupons are useful for exploring local deformation and failure processes within the braided composite material and

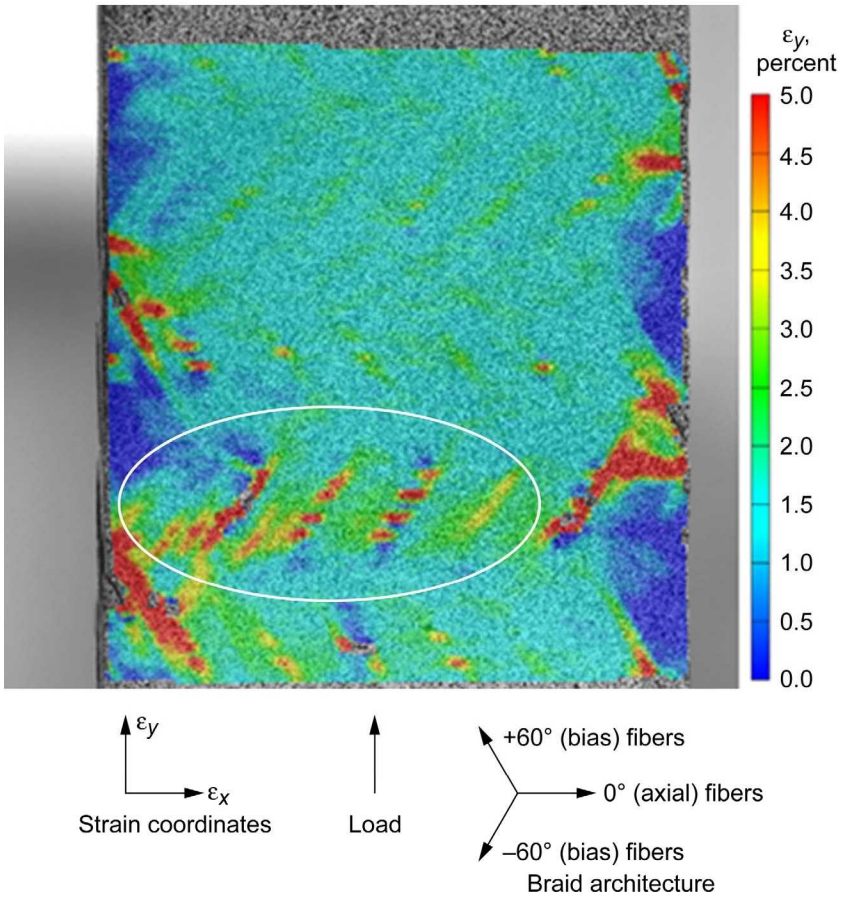

Figure 11.—Example of fiber bundle splitting and edge delamination in T700S/PR520 transverse tensile specimen at load close to ultimate load.

for providing an estimate of the global stress-strain response. The circled area in Figure 11 shows a large number of subsurface axial fiber bundle splits (horizontal red lines) for a load close to ultimate failure strength. Figures 12 and 13 show axial surface strains for the T700S/PR520 and T700S/5208 material systems at loads sufficient to initiate only a small number of such subsurface axial fiber bundle splits. The load required to initiate these splits is higher for the toughened T700S/PR520 material system (Fig. 12) than for the untoughened T700S/5208 material system (Fig. 13).

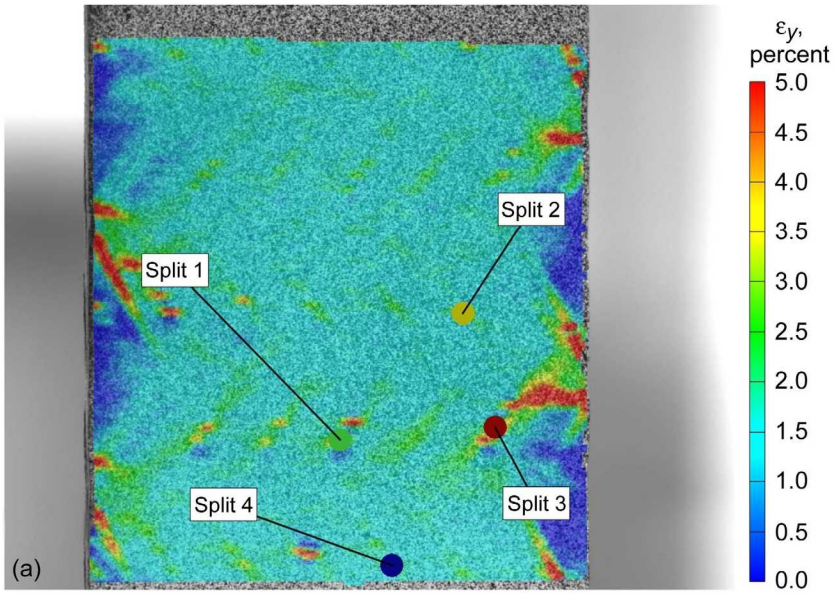

Global strain: 1.57 percent
Global stress: 574 MPa (83 ksi)

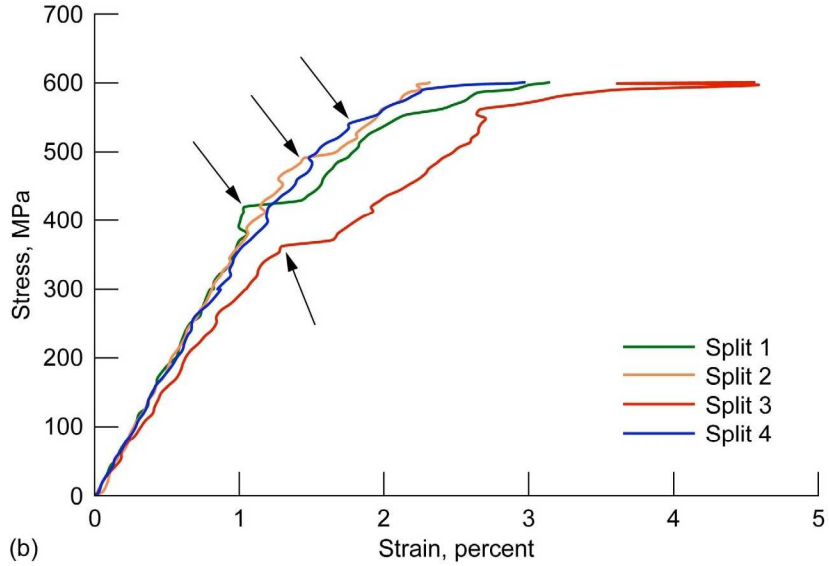

Figure 12.—Example of fiber bundle splitting for toughened T700S/PR520 material system. (a) Full-field axial strain (ε_y) data. (b) Global stress versus local strain plot. Arrows indicate local strains at onset of splitting.

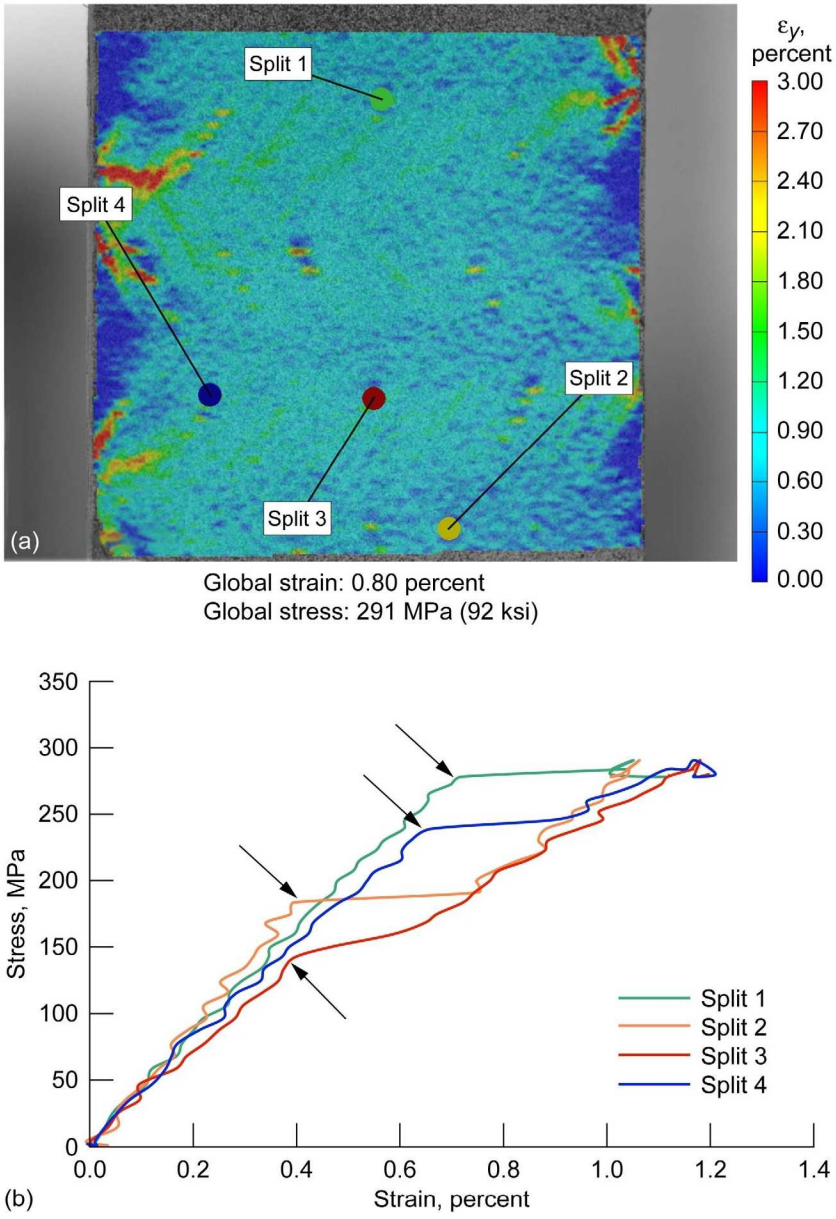

Figure 13.—Example of fiber bundle/matrix system splitting for untoughened T700S/5208 material system. (a) Full-field axial strain (ε_y) data. (b) Global stress versus local strain plot. Arrows indicate local strains at onset of splitting.

Global stress-local strain curves are plotted at the locations of four split sites for each material system. Figure 12(a) shows the four split locations used for the T700S/PR520 material, and Figure 12(b) shows the corresponding global stress-local strain curves at each of the four split locations. A sudden increase in strain without a significant increase in stress indicates that a fiber bundle split has occurred. The local strains at the onset of splitting are indicated by arrows in Figure 12(b). Prior to splitting, the global stress-local strain curves in Figure 12(b) are similar to the global stress-global strain curve in Figure 3. After splitting has occurred the local strain measurement may no longer be accurate because of large distortions in the speckle pattern. The strain at the onset of splitting (indicated by the arrows in Fig. 12(b)) is the in situ fiber bundle transverse failure strain for the 0° braid fibers. For the four points used in Figure 12, the mean value of transverse failure strain is approximately 1.4 percent, with values ranging from 1.0 to

1.8 percent. The value of global stress at which the first fiber bundle failed in Figure 12(b) is approximately 350 MPa. This is close to the stress at which the transverse global stress-global strain curve in Figure 3 becomes nonlinear. This suggests that transverse fiber bundle failures are one possible cause for the nonlinear behavior. However, the edge effects discussed above could also be contributing to the nonlinear response.

Figure 13(a) shows the four split locations used for the untoughened T700S/5208 material, and Figure 13(b) shows the corresponding global stress-local strain curves at each of the four split locations. Results for the T700S/5208 material system are similar to those presented for the T700S/PR520 material system except that the sudden increase in strain associated with fiber bundle splitting is more pronounced and occurs at a lower strain. Prior to splitting, the global stress-local strain curves in Figure 13(b) are similar to the global stress-global strain curve in Figure 4. For the four points used in Figure 13, the mean value of transverse failure strain is approximately 0.5 percent with values ranging from 0.4 to 0.7 percent. The value of global stress at which the first fiber bundle failed in Figure 13(b) is approximately 140 MPa. This is close to the stress at which the transverse global stress-global strain curve in Figure 4 becomes nonlinear. Edge effects are also significant for the T700S/5208 material system. For both material systems fiber bundle splitting initiates well below the ultimate global stress values indicated in Figures 3 and 4 and in Table III. Between the initiation of fiber bundle splitting and overall composite failure, the fiber bundle splits are growing and propagating throughout the composite. Once damage accumulation reaches a critical value, the composite fails. This accumulation of damage is one possible explanation for the nonlinear response and the reduced tensile strength for the transverse tensile properties compared with the axial tensile properties shown in Figures 3 to 5. Further work using modified specimen designs and testing of larger structures is needed to determine if the reduced tensile strength is a real material property or a result of edge damage in the straight-sided specimens.

Local Deformation in Axial Tensile Tests

Figure 7 shows that splitting of bias fibers occurs in axial tensile tests. In axial tensile tests the 0° fiber bundles extend through the specimen and are gripped by the test fixtures. Since most of the load is carried by the axial fibers, splitting of bias fiber bundles does not have a large effect on the measured stiffness, and the global stress-global strain curves in Figures 3 to 5 are nearly linear until close to failure. However, there is a significant difference in axial tensile strength between the toughened and untoughened material systems. The development of bias fiber bundle splits as the axial tensile specimens are loaded is shown in Figure 14. Axial surface strains are shown at three different load conditions for each material in order to examine: (1) the onset of fiber bundle splitting, (2) the extent of fiber bundle splitting at a common stress value, and (3) the extent of fiber bundle splitting at the last data point collected before failure.

The onset of bias fiber bundle splitting occurs at a very low strain of 0.28 percent for the untoughened T700S/5208 material system compared with 0.90 percent for the toughened T700S/PR520 material system. This is consistent with the lower strength of the 5208 resin compared to the PR520 resin shown in Table II. However, low fiber/matrix interface strength could also lead to reduced transverse fiber bundle strength. Further work is needed to identify the mechanism for initiation of the splits. Regardless of the cause, the untoughened system shows a lower initiation stress for bias fiber bundle splitting and much more spitting at equal load compared with the toughened system. The ultimate strain for the toughened system is 2.21 percent, which is nearly the same as the expected failure strain of the fiber. Although some bias fiber bundle splitting is observed in Figure 14 for T700S/PR520, the splitting does not limit the load carrying capability of the axial fibers. In contrast, the extensive bias fiber bundle splitting for T700S/5208 limits the strain capability of the axial fibers either directly by inducing local strain concentrations or indirectly by allowing additional damage to propagate from the splits.

Some out-of-plane deformation was observed in the axial tensile tests. In Figure 15 the out-of-plane deformation is shown for four specimens of the T700S/E–862 material system when loaded in an axial tensile test to four different percentages of ultimate load (25, 50, 75, and 90 percent). After the

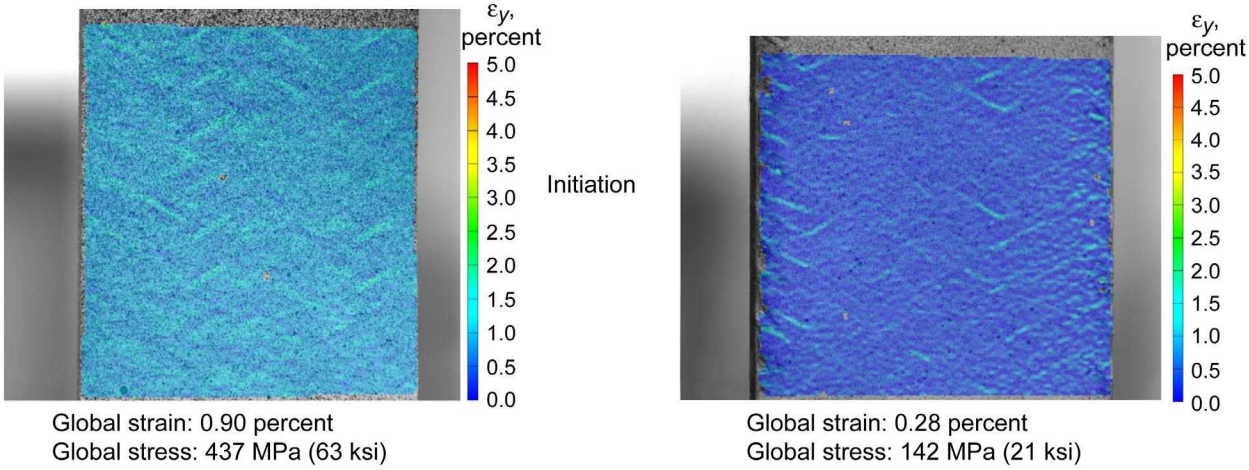

Figure 14.—Axial strain (ε_y) time histories for toughened and untoughened material systems. (a) T700S/PR520 (toughened). (b) T700S/5208 (untoughened).

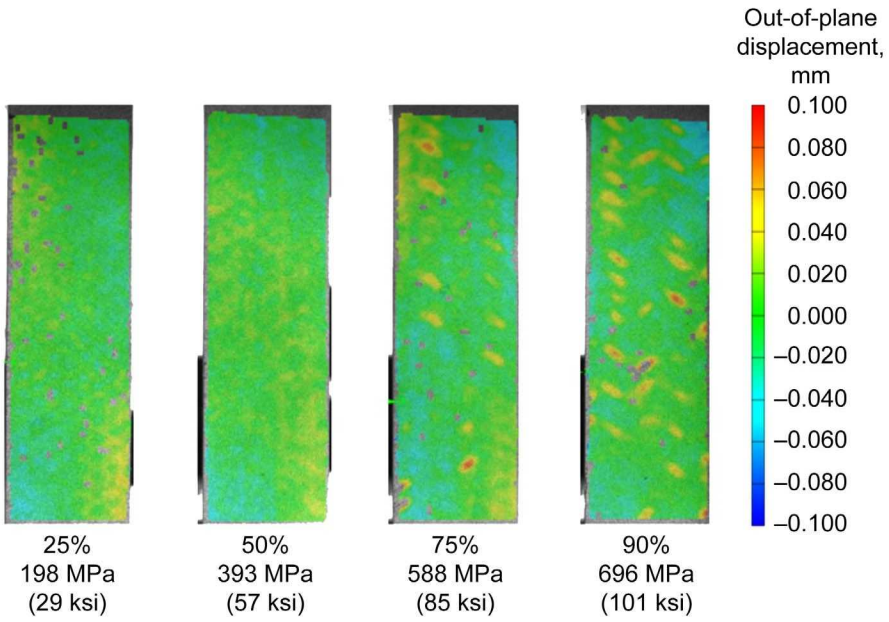

Figure 15.—Out-of-plane displacements for T700S/E–862 material system at various percentages of ultimate load.

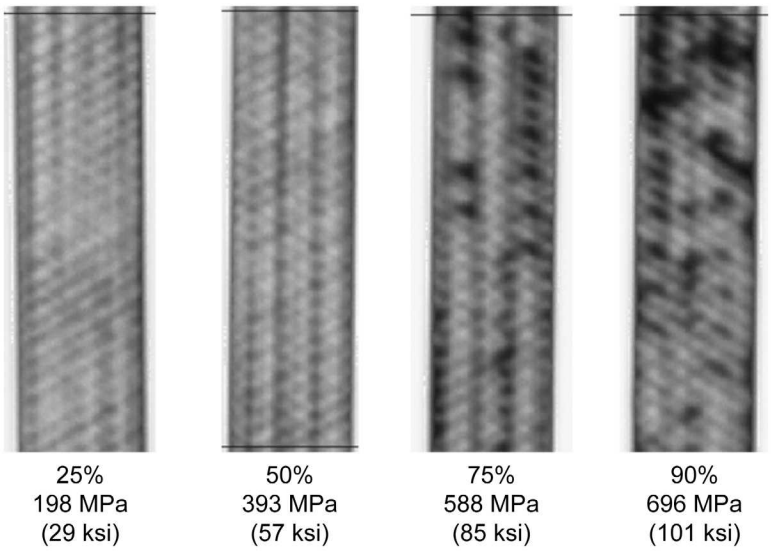

Figure 16.—Ultrasonic through transmission scans for T700S/E–862 axial tests at various percentages of ultimate load.

load-unload cycles the specimens were examined by ultrasonic through transmission (UTT) and microscopy. At 75 percent of ultimate load, distinct areas of out-of-plane deformation are visible as yellow or as yellow and red regions oriented along the bias fiber directions. This out-of-plane deformation could be a result of straightening of undulating axial fibers, local delamination between crossing fiber bundles, or damage within fiber bundles. Preliminary microscopy results indicated that some areas exhibiting large out-of-plane displacements also had local delamination, but more microscopic evaluation is needed for conclusive results.

The UTT results are shown in Figure 16 for the same specimens used for Figure 15. There is good correlation between the localized regions of out-of-plane deformation in Figure 15 and areas of reduced transmission indicated as dark regions in the UTT data in Figure 16. In Figure 16 there are only normal

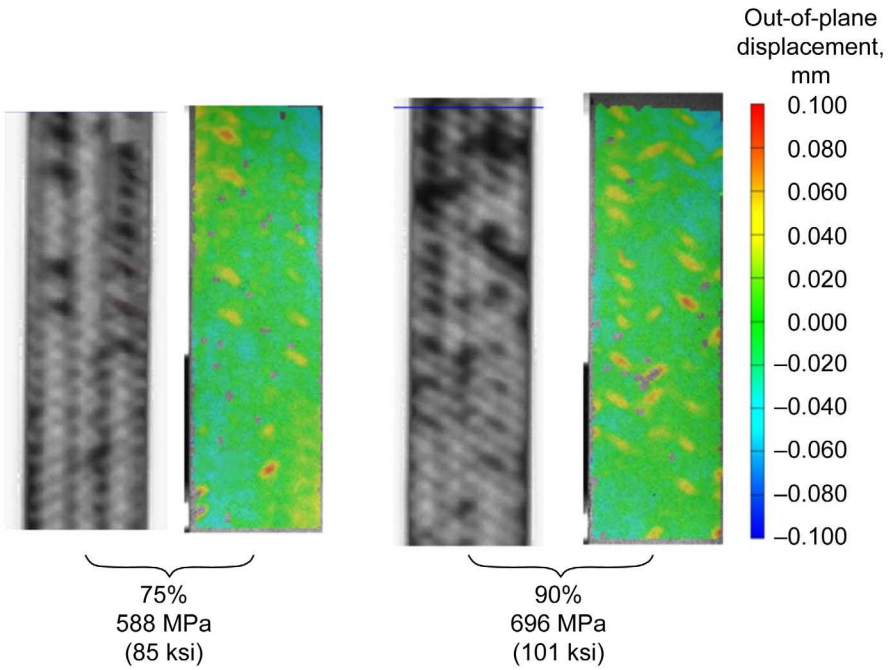

Figure 17.—Ultrasonic through transmission and optical measurements for T700S/E–862 specimens loaded to 75 and 90 percent of ultimate load.

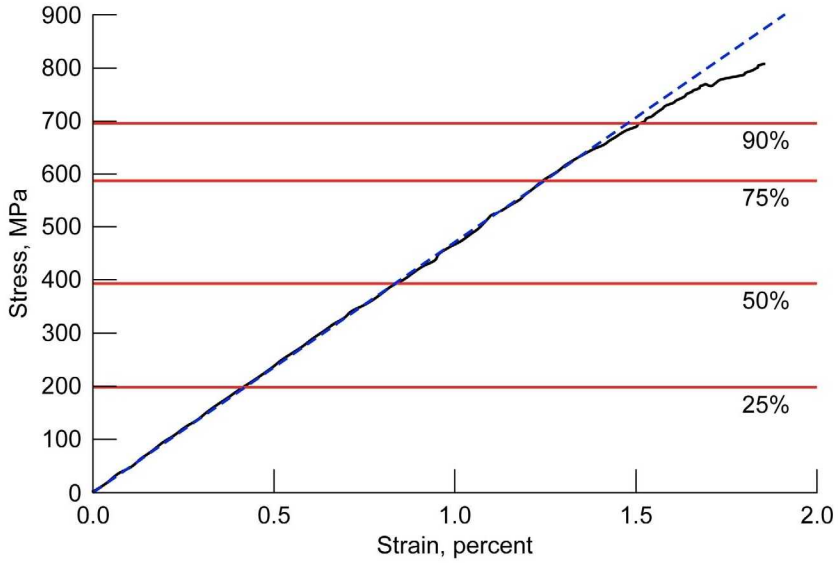

Figure 18.—T700S/E–862 stress-strain curve noting the four stress levels indicated in Figures 15 to 17.

variations in the braid pattern for specimens loaded to 25 and 50 percent of the ultimate load. However, specimens loaded to 75 and 90 percent of ultimate show dark regions of reduced transmission indicating possible local delamination or other damage. The patterns for out-of-plane deformation and through transmission intensity are compared in Figure 17 for specimens loaded to 75 and 90 percent of ultimate.

Figure 18 shows 25, 50, 75, and 90 percent load levels on the global stress-strain curve for an axial tensile test of a T700S/E–862 specimen tested to failure. The solid black curve is the test data, and the dashed blue line is used to check for linearity. The stress-strain curve becomes nonlinear at strains above

75 percent. It appears that bias fiber bundle splitting at low strains has little effect on the global stress-strain curve, but accumulated splitting, local delamination, or other local damage contribute to global nonlinearity at high strains.

Conclusions

Digital image correlation techniques were used to examine the local strain field in triaxial braid composites under tensile loading. An overlay of the full-field surface strain on a digital image of the composite surface was useful for identifying the location of local damage with respect to the braid architecture. In transverse tensile tests the types of local damage observed were splitting within the subsurface 0° fiber bundles and edge delamination. The strain at which these local damage events initiated correlated with the strain at which the global stress-strain curve became nonlinear. The in situ transverse failure strain for the 0° fiber bundles was determined by measuring the global stress versus local strain at sites where splitting occurred. Use of a toughened resin system delayed the onset of the local damage events and reduced the extent of damage. As a result, the global stress-strain curves were linear to a higher strain level, and the ultimate strain and ultimate load were higher for the toughened material system. In axial tensile tests the types of local damage observed were splitting within the surface bias fiber bundles at low strains followed by local delamination and damage as the strain approached the ultimate strain. In contrast to the transverse tensile tests, these local damage events did not cause a large deviation from linearity because the axial tensile load is carried mostly by the 0° fiber bundles. The local damage did cause a reduction in the ultimate failure strain for the composite when untoughened resins were used. This reduction in ultimate strain occurs because the local damage causes stress concentrations around the 0 fiber bundles that are carrying most of the load. For the toughened material system there was much less local damage, and the axial tensile failure strain of the composite was nearly the same as that of the fiber. Further work is needed to fully understand the role of matrix properties and fiber/matrix interface properties on the onset and accumulation of local damage. Further work is also needed to develop reliable test methods that can overcome the problem of edge effects when standard straight-sided coupons are used to test large-unit-cell-size triaxial braid composites.

References

1. Standard Test Method for Tensile Properties of Polymer Matrix Composite Materials. ASTM D3039, ASTM International, West Conshohocken, PA, 2006.
2. Composite Materials Handbook. MIL–HDBK–17–1F, Defense Technical Information Center, 2002.
3. Tomblin, John S.; Ng, Yeow C.; and Raju, K.S.: Material Qualification and Equivalency for Polymer Matrix Composite Material Systems. DOT/FAA/AR–00/47, Federal Aviation Administration, Washington, DC, 2001.
4. Tomblin, J., et al.: Material Qualification Methodology for 2×2 Biaxially Braided RTM Composite Material Systems. AGATE–WP3.3–033048–116, 2001.
5. Masters, John E., et al.: The Effects of Specimen Width on Tensile Properties of Triaxially Braided Textile Composites. Third NASA Advanced Composites Technology Conference, vol. 1, no. 2, Washington, DC, 1993, pp. 523–536.
6. Masters, John E.: Strain Gage Selection Criteria for Textile Composite Materials. NASA CR–198286, 1996.
7. Masters, John E.; and Portanova, Marc A.: Standard Test Methods for Textile Composites. NASA CR– 4751, 1996.
8. Masters, John E.; and Ifju, Peter G.: A Phenomenological Study of Triaxially Braided Textile Composites Loaded In Tension. Comp. Sci. T., vol. 56, no. 3, 1996, pp. 347–358.
9. Tsotsis, Thomas K., et al.: Towards Rapid Screening of New Composite Matrix Resins. Comp. Sci. T., vol. 66, nos. 11–12, 2006, pp. 1651–1670.

10. Grediac, Michel: The Use of Full-Field Measurement Methods in Composite Material Characterization: Interest and Limitations. Composites Part A: Applied Science and Manufacturing, vol. 35, nos. 7–8, 2004, pp. 751–761.
11. Gliesche, Konrad, et al.: Investigations of In-Plane Shear Properties of ±45°-Carbon/Epoxy Composites Using Tensile Testing and Optical Deformation Analysis. Comp. Sci. T., vol. 65, no. 2, 2005, pp. 163–171.
12. Pindera, M.J; Ifju, P.; and Post, D.: Iosipescu Shear Characterization of Polymeric and Metal Matrix Composites. Exper. Mech., vol. 30, no. 1, 1990, pp. 101–108.
13. Hale, R.D.: An Experimental Investigation Into Strain Distribution in 2D and 3D Textile Composites. Comp. Sci. T., vol. 63, 2003, pp. 2171–2185.
14. Hubner J.P., et al.: Luminescent Photoelastic Coatings. Exper. Mech., vol. 44, no. 4, 2004, pp. 416–424.
15. Fergusson, A.D., et al.: Flexural Testing of Composite Sandwich Structures With Digital Speckle Photogrammetry. Applied Mechanics and Materials, vols. 5–6, 2006, pp. 135–144.
16. Littell, Justin D., et al.: Measurement of Epoxy Resin Tension, Compression, and Shear Stress-Strain Curves Over a Wide Range of Strain Rates Using Small Test Specimens. J. Aerospace Eng. Sp. Issue—Impact Mechanics and High Energy Absorption Materials, vol. 21, no. 3, 2008, pp. 162–173.
17. Littell, Justin D.: The Experimental and Analytical Characterization of the Macromechanical Response for Triaxial Braided Composite Materials. Ph.D. dissertation, Univ. of Akron, Akron, OH, 2008. http://www.ohiolink.edu/etd/view.cgi?acc_num=akron1224164770
18. GOM Optical Measuring Techniques. Industrial 3D Measurement Techniques, 2009. www.gom.com Accessed Mar. 20, 2009.

REPORT DOCUMENTATION PAGE		Form Approved OMB No. 0704-0188

The public reporting burden for this collection of information is estimated to average 1 hour per response, including the time for reviewing instructions, searching existing data sources, gathering and maintaining the data needed, and completing and reviewing the collection of information. Send comments regarding this burden estimate or any other aspect of this collection of information, including suggestions for reducing this burden, to Department of Defense, Washington Headquarters Services, Directorate for Information Operations and Reports (0704-0188), 1215 Jefferson Davis Highway, Suite 1204, Arlington, VA 22202-4302. Respondents should be aware that notwithstanding any other provision of law, no person shall be subject to any penalty for failing to comply with a collection of information if it does not display a currently valid OMB control number.
PLEASE DO NOT RETURN YOUR FORM TO THE ABOVE ADDRESS.

1. REPORT DATE *(DD-MM-YYYY)*	2. REPORT TYPE	3. DATES COVERED *(From - To)*
01-05-2009	Technical Memorandum	

4. TITLE AND SUBTITLE
Characterization of Damage in Triaxial Braid Composites Under Tensile Loading

5a. CONTRACT NUMBER

5b. GRANT NUMBER

5c. PROGRAM ELEMENT NUMBER

6. AUTHOR(S)
Littell, Justin, D.; Binienda, Wieslaw, K.; Roberts, Gary, D.; Goldberg, Robert, K.

5d. PROJECT NUMBER

5e. TASK NUMBER

5f. WORK UNIT NUMBER
WBS 698259.02.07.03.04.01

7. PERFORMING ORGANIZATION NAME(S) AND ADDRESS(ES)
National Aeronautics and Space Administration
John H. Glenn Research Center at Lewis Field
Cleveland, Ohio 44135-3191

8. PERFORMING ORGANIZATION REPORT NUMBER
E-16897-1

9. SPONSORING/MONITORING AGENCY NAME(S) AND ADDRESS(ES)
National Aeronautics and Space Administration
Washington, DC 20546-0001

10. SPONSORING/MONITORS ACRONYM(S)
NASA

11. SPONSORING/MONITORING REPORT NUMBER
NASA/TM-2009-215645

12. DISTRIBUTION/AVAILABILITY STATEMENT
Unclassified-Unlimited
Subject Category: 24
Available electronically at http://gltrs.grc.nasa.gov
This publication is available from the NASA Center for AeroSpace Information, 301-621-0390

13. SUPPLEMENTARY NOTES

14. ABSTRACT
Carbon fiber composites utilizing flattened, large tow yarns in woven or braided forms are being used in many aerospace applications. Their complex fiber architecture and large unit cell size present challenges in both understanding deformation processes and measuring reliable material properties. This report examines composites made using flattened 12k and 24k standard modulus carbon fiber yarns in a 0°/+60°/-60° triaxial braid architecture. Standard straight-sided tensile coupons are tested with the 0° axial braid fibers either parallel with or perpendicular to the applied tensile load (axial or transverse tensile test, respectively). Nonuniform surface strain resulting from the triaxial braid architecture is examined using photogrammetry. Local regions of high strain concentration are examined to identify where failure initiates and to determine the local strain at the time of initiation. Splitting within fiber bundles is the first failure mode observed at low to intermediate strains. For axial tensile tests splitting is primarily in the ±60° bias fibers, which were oriented 60° to the applied load. At higher strains, out-of-plane deformation associated with localized delamination between fiber bundles or damage within fiber bundles is observed. For transverse tensile tests, the splitting is primarily in the 0° axial fibers, which were oriented transverse to the applied load. The initiation and accumulation of local damage causes the global transverse stress-strain curves to become nonlinear and causes failure to occur at a reduced ultimate strain. Extensive delamination at the specimen edges is also observed.

15. SUBJECT TERMS
Composite materials; Braided composites; Graphite-epoxy composites

16. SECURITY CLASSIFICATION OF:			17. LIMITATION OF ABSTRACT	18. NUMBER OF PAGES	19a. NAME OF RESPONSIBLE PERSON
a. REPORT	b. ABSTRACT	c. THIS PAGE			STI Help Desk (email:help@sti.nasa.gov)
U	U	U	UU	25	19b. TELEPHONE NUMBER *(include area code)* 301-621-0390